



OPEN Decontamination of crystal violet using nanocomposite adsorbent based on pine cone biochar modified with $\text{CoFe}_2\text{O}_4/\text{Mn-Fe}$ LDH

Seyed Jamaledin Peighambardoust^{1✉}, Shima Abdollahian Aghbolagh¹, Rauf Foroutan¹ & Naeimeh Sadat Peighambardoust²

This study investigates the use of pine cones as a novel and readily available precursor for producing biochar (BC), which is then modified with CoFe_2O_4 magnetic nanoparticles and Mn-Fe layered double hydroxide (LDH) to enhance its adsorption capacity for removing the cationic dye crystal violet (CV) from aqueous solutions. The physical and chemical properties of the resulting adsorbents—BC (BCPC), BC/ CoFe_2O_4 , and BC/ $\text{CoFe}_2\text{O}_4/\text{Mn-Fe}$ LDH—were characterized using FTIR, XRD, VSM, SEM, EDX mapping, and BET analyses. BET results revealed that the specific surface areas of BCPC, BCPC/ CoFe_2O_4 , and BCPC/ $\text{CoFe}_2\text{O}_4/\text{Mn-Fe}$ LDH were 43.41, 95.81, and 98.85 m^2/g , respectively, indicating a significant enhancement in surface area due to modification. Additionally, the magnetic saturation of the BCPC/ $\text{CoFe}_2\text{O}_4/\text{Mn-Fe}$ LDH composite was 32.35 emu/g, confirming that the composite could be easily separated from the solution using an external magnetic field. The composite achieved a maximum CV dye removal efficiency of 98.54% under optimal conditions: pH=9, temperature 25 °C, adsorbent dose of 1 g/L, contact time of 70 min, and initial dye concentration of 10 mg/L. Isotherm studies revealed that the Langmuir model provided the best fit for the experimental data, suggesting a monolayer adsorption process on homogeneous surfaces. Kinetic studies indicated that the pseudo-second-order model was the most appropriate, highlighting the importance of chemical interactions in the adsorption process. Thermodynamic analyses revealed that the adsorption process was exothermic and spontaneous, as confirmed by negative enthalpy (ΔH°) and Gibbs free energy (ΔG°) values. In contrast, the negative entropy (ΔS°) indicated a reduction in randomness during adsorption. This study demonstrates that the BCPC/ $\text{CoFe}_2\text{O}_4/\text{Mn-Fe}$ LDH magnetic nanocomposite is an effective, sustainable, and easily separable adsorbent for removing cationic dyes from aqueous environments.

Keywords Cationic dye, Aqueous solution, Layered double hydroxide, Magnetic composite, Biochar

Water is a vital substance for all living organisms and plays an essential role in the progress of human civilization and its use in various sectors such as industry and agriculture¹. Unfortunately, due to population growth and rapid industrialization, pollution of freshwater resources by multiple pollutants, such as textile dyeing agents, pesticides, heavy metals, pharmaceutical compounds, etc., has become a critical and dangerous issue². Among these pollutants, dyes are widely used in various industries such as fabric dyeing, leather industry, food, etc³. The textile industry ranks among the highest in water consumption and releases considerable quantities of wastewater containing organic dyes into surface water bodies⁴. Around 800,000 tons of dyes are produced yearly, with approximately 140,000 tons lost due to inefficient fabric binding⁵. Cationic dyes are hazardous because they can cause various severe diseases among different groups of dyes. One of the most essential cationic dyes is crystal violet (CV)⁶, which contains quaternary ammonium groups. The nitrogen atom is bonded to four alkyl groups, creating a net positive charge. This property increases the solubility of CV in water and leads to health complications such as liver and kidney diseases, respiratory failure, skin irritation, genetic mutations, cancer, and coronary infarction^{7,8}. Consequently, its removal from aqueous solutions is essential and critical.

Various methods have been proposed for removing color-forming pollutants from aqueous solutions, divided into three general categories: physical, chemical, and biological⁹. The adsorption technique is a type of physical

¹Faculty of Chemical and Petroleum Engineering, University of Tabriz, Tabriz 5166616471, Iran. ²Koç University Boron and Advanced Materials Application and Research Center (KUBAM), Sariyer 34450, Istanbul, Turkey. ✉email: j.peighambardoust@tabrizu.ac.ir

method that has always attracted the attention of researchers due to its efficiency, selectivity, low operating cost¹⁰, selective process, simplicity¹¹, flexibility, and low cost^{12,13}. In this method, the use of low-cost adsorbents with high surface area and adsorption capacity has always attracted the attention of researchers, including activated carbon, zeolite, silica, carbon nanotubes, polymers, biochar, industrial waste, clay, and agricultural waste^{14,15}. Using agricultural waste as an adsorbent reduces its natural accumulation and the cost of producing efficient and effective adsorbents for removing pollutants from aqueous solutions¹⁶. Biochar (BC) is produced by the thermal decomposition of biomass and agricultural and animal wastes in an oxygen-free environment. It is characterized by desirable properties such as high specific surface area, functional groups on its surface, and its porous structure^{17,18}. Pine trees are highly valued worldwide for their wood, contributing significantly to the economy. Consequently, a substantial amount of pine cones accumulates in the environment without a specific use. Composed of hemicellulose (46.5%), cellulose (18.8%), and lignin (37.4%), pine cones present an appealing and cost-efficient raw material for the production of biochar (PCBC)¹⁹. Furthermore, pine cones are a suitable and low-cost option for biochar production due to their renewable nature, abundance, availability, and economic cost²⁰.

Layered double hydroxides (LDHs) are materials belonging to the hydrotalcite group, which consist of two layers of divalent and trivalent metal cations (Mn, Al, Ca, Fe) and anions (hydroxides, carbonates, chlorides), which are interconnected by electrostatic interactions^{21,22}. These materials' essential advantages and features include good ion exchange capacity, high specific surface area, low toxicity, reversibility of the structure, and simple and cost-effective synthesis methods^{23,24}. However, to prevent the aggregation of LDHs, they can be loaded onto a cost-effective and stable particle matrix such as BC. This approach reduces the aggregation of LDHs, increases the existence of functional groups on the surface of the BC, and provides a larger reaction area^{24,25}. However, despite the high dye adsorption capacity of LDHs, traditional processes such as filtration and centrifugation pose a significant challenge in the separation process and limit the use of adsorbents²⁶. Therefore, magnetic field-based separation technology can effectively separate powdered adsorbents from aqueous solutions and potentially enhance dye adsorption²⁷. Cobalt ferrite (CoFe_2O_4) is a material with moderate saturation magnetism suitable for adsorption due to its strong mechanical strength and good chemical stability^{28–30}.

The present study used pine cones as a suitable and available product for producing activated carbon. Then, it was modified using CoFe_2O_4 and Mn-Fe LDH using chemical precipitation. After the modification of BC prepared from a pine cone, the adsorption ability of BC, BC/ CoFe_2O_4 , and BC/ CoFe_2O_4 @Mn-Fe LDH samples was investigated by removing cationic CV dye from an aqueous solution. In this study, various analyses were used to characterize the physical and chemical properties of the selected adsorbents. The impact of temperature, pH, contact time, adsorbent dosage, and initial CV dye concentration on the adsorption efficiency was examined. Additionally, kinetic, thermodynamic, and isotherm studies were conducted to explore the adsorption process. The process was further analyzed regarding its physical, chemical, and exothermic/endothermic behavior.

Materials and methods

Materials and equipment

In the present study, pine cones obtained from the campus of Tabriz University were used as raw materials for biochar production. Anhydrous ferric chloride (FeCl_3 , MW: 162.2 g/mol) was purchased from Pharmachemical Company, Iran, hexahydrate cobalt nitrate ($\text{Co}(\text{NO}_3)_2 \cdot 6\text{H}_2\text{O}$, MW: 291.04 g/mol), hexahydrate cobalt nitrate ($\text{MnCl}_2 \cdot 4\text{H}_2\text{O}$, MW: 197.91 g/mol), sodium hydroxide (NaOH , MW: 40 g/mol), hydrochloric acid (HCl , Purity: 37%) were purchased and used from Merck Company.

To investigate the structural properties, FTIR, SEM, BET, XRD, and EDX-Map techniques were used, and the specifications of the devices have been fully presented in previous reviews³¹. A UV-vis instrument, Specord 250, manufactured by Analytik Jena, was used to examine the concentration of the residual CV dye in the aqueous solution. Also, to explore the magnetic properties of the samples, a VSM instrument, LBKFB, manufactured by Kashan Desert Magnetis Company, was used.

Adsorbents' synthesis

This study used pine cones from the University of Tabriz campus fruit of pine trees to prepare biochar. Initially, the collected cones were washed with water several times to remove impurities. After washing, the cones were placed at 70 °C for 24 h to dry completely. After drying, the cones were placed in a tube furnace under a nitrogen atmosphere at 500 °C for 3 h to carbonize completely. The carbonized cones were ground into powder using a mill to synthesize the desired composites. To surface modify pine cone carbon with magnetic cobalt ferrite nanoparticles CoFe_2O_4 by chemical precipitation method, 1.35 g of iron (III) chloride and 0.6 g of cobalt (II) nitrate (molar ratio of iron to cobalt 2:1) in 50 mL of water were stirred in a flask for 10 min at room temperature by magnetic stirring (500 rpm) until completely dissolved. In the next step, 0.5 g of pine cone carbon was added and stirred for 20 min with magnetic stirring (500 rpm). The mixture was stirred in an oil bath at 80–90 °C. In another beaker, 3 g of sodium hydroxide was added dropwise to 50 mL of distilled water and stirred for 10 min to homogenize. After that, 3 M sodium hydroxide solution was added to the flask as an oxidant and stirred for 3 h at the same temperature and 500 rpm to complete the reaction. Following the reaction, a magnet was used to separate the synthesized magnetic nanocomposite from the water, which was then washed multiple times with distilled water to neutralize the pH (6–7). Once neutralized, the nanocomposite was placed in an oven at 100 °C for 24 h to achieve thorough drying. A pine cone carbon surface modified with magnetic cobalt ferrite nanoparticles (BC/ CoFe_2O_4) was used at this stage.

In the next step, to synthesize the BC/ CoFe_2O_4 @Mn-Fe LDH magnetic nanocomposite via the chemical precipitation method, 0.811 g of ferric chloride and 0.989 g of manganese chloride (molar ratio of iron to manganese 1:1)³¹ were dissolved in 50 mL of water and stirred with 500 rpm for 10 min at room temperature using a magnetic stirrer until a homogeneous solution was achieved. Then, 0.7 g of BC/ CoFe_2O_4 was added to

the mixture, and stirring continued at 500 rpm for another 30 min. In a separate container, 0.7 g of NaOH and 0.75 g of sodium carbonate were dissolved in 50 mL of distilled water and stirred for 10 min until thoroughly mixed. Finally, 50 mL of the above solution was added to the flask and stirred for 4 h at 65 °C to complete the reaction. After the reaction, it was washed with distilled water using a centrifuge (2500 rpm and 5 min) to neutralize it completely. Finally, it was dried in an oven at 100 °C for 24 h. It is worth noting that in the structure of the BC/CoFe₂O₄@Mn-Fe LDH sample, the ratio of Biochar: Mn-Fe LDH: CoFe₂O₄ is 1:0.5:0.5.

Study of the dye adsorption process

A 1,000 mg/L stock solution of CV dye was prepared by dissolving 1 g of CV dye in 1 L of distilled water. This stock solution was then diluted with distilled water to produce samples of different concentrations for the adsorption experiments. The adsorption process of CV dye was conducted in a batch system using BC, BC/CoFe₂O₄, and BC/CoFe₂O₄@Mn-Fe LDH samples. The effects of temperature (25–50 °C), contact time (5–100 min), pH (2–9), pollutant concentration (10–50 ppm), and adsorbent dose (0.5–4 g/L) on the adsorption process were evaluated. An aqueous solution of CV dye was initially prepared to examine the impact of pH on dye removal. The pH was subsequently adjusted using 0.1 M NaOH and HCl solutions. A specific amount of adsorbent was added and stirred for a set duration using a magnetic stirrer. Finally, the adsorbents were separated from the solution by centrifugation. The adsorption efficiency and capacity were determined using Eqs. 1 and 2, respectively:

$$q_e = (C_i - C_e) \times \frac{V}{m} \quad (1)$$

$$R(\%) = \frac{(C_i - C_e)}{C_i} \times 100 \quad (2)$$

In these equations, C_i and C_e (mg/g) represent the CV dye's initial and equilibrium concentrations in the solution, respectively. W (g) is the weight of the adsorbent used, and V (L) is the volume of the aqueous solution. After optimizing the mentioned parameters, further studies were carried out to examine the kinetic, thermodynamic, and equilibrium behaviors of the CV dye adsorption process and the effect of counter ions.

Results and discussion

Adsorbent properties

Figure 1a shows the FTIR analysis to determine the functional groups for BC, BC/CoFe₂O₄, and BC/CoFe₂O₄@Mn-Fe LDH samples. In the structure of the prototype BC sample, the absorption peaks at wavenumbers of 3,433 and 1,073 cm⁻¹ are related to O-H stretching³². Also, other absorption peaks in the 2,861–2,959 cm⁻¹ range are related to the -CH₂ group³³. The single absorption peak at 1,728 cm⁻¹ is also assigned to the C=O stretching vibration associated with the ester group in hemicellulose³⁴. Meanwhile, the absorption peaks at 1,460 and 1,383 cm⁻¹ are linked to the C-C³⁵ and aromatic C=C stretching vibrations³⁶. Moreover, the peak at 1278 cm⁻¹ is attributed to the C=O stretching in ethers, alcohols, and/or phenols³⁶. After modification of BC using CoFe₂O₄ nanoparticles, the peak observed at 1,382 cm⁻¹ represents the Co-O-Fe vibrations, and the wavenumber of 802 cm⁻¹ represents the Fe-O vibrations. Furthermore, the absorption peak at 589 cm⁻¹ is attributed to the stretching vibrations of the metal-oxygen bonds in the tetrahedral and octahedral sites of the spinel lattice in ferrite compounds³⁷. The FTIR spectrum of the BC/CoFe₂O₄ sample displays characteristic absorption peaks of CoFe₂O₄ nanoparticles, confirming their presence on the biochar surface. In the BC/CoFe₂O₄@Mn-Fe LDH sample, the absorption peaks in the 500–1,000 cm⁻¹ range correspond to vibrational modes associated with metal-oxygen (M-O) or metal-hydroxyl (M-OH) group vibrations, likely representing Fe-OH, Mn-OH, Fe-O, and Mn-O bonds^{38,39}. In addition, the sharp absorption peak at 1,439 cm⁻¹ could indicate the vibrational absorption of CO₃²⁻ within the interlayers⁴⁰. The results in Fig. 1b showed that following the CV dye adsorption process, the intensity and position of the absorption peaks changed somewhat, indicating their interaction with the dye molecules, confirming the adsorption of CV dye to the adsorbent surface via van der Waals forces⁴¹. It is worth noting that the magnitude of the changes was not significant. However, in the BC/CoFe₂O₄@Mn-Fe LDH-dye sample, a new absorption peak appeared at 1,117 cm⁻¹, possibly due to the C-H stretching vibrations in the aromatic ring⁴². It is important to note that the precise identification of the functional groups related to each of the adsorbent components is impossible using FTIR analysis due to the overlap of some peaks. Therefore, other techniques and analyses were used for precise identification.

Figure 1c shows the XRD spectra to investigate the amorphous and crystalline structures and also to determine the structural properties of BC, Mn-Fe LDH, BC/CoFe₂O₄, BC/Mn-Fe LDH, and BC/CoFe₂O₄@Mn-Fe LDH samples. In the BC sample, broad peaks in the 10–30° range are observed, corresponding to the (002) crystalline phase and showing the amorphous nature of the BC sample⁴⁴. The absence of sharp peaks suggests that this sample exhibits an amorphous structure. Additionally, in the Mn-Fe LDH structure, peaks of varying intensities are observed in the range of 24.36, 31.44, 37.56, 41.56, and 51.72°, which are attributed to the (012), (104), (110), (113), (202) and (018) crystalline phases, respectively⁴¹. In addition, two peaks in the 31.4 and 51.6° range have appeared in the Mn-Fe LDH sample structure, which is assigned to the (020) and (251) crystalline phases in the Mn(OH)O and FeOOH structures, respectively, based on PDF#74–1049 and PDF#75–1594⁴⁵. In the BC/CoFe₂O₄ sample, two crystalline and amorphous parts are observed. The amorphous part can be related to BC. The peaks observed in the crystalline part in the ranges of 30.14, 35.38, 43.22, 57.12, and 62.6° can be attributed to the crystalline phases (220), (311), (400), (511) and (440), respectively, which indicate the primary material of the CoFe₂O₄ spinel structure (JCPDS no 22–1086)⁴⁶. On the other hand, in the BC/Mn-Fe LDH sample, peaks in the range of 31.28 and 51.5° are observed, which indicates the proper placement of Mn-Fe LDH in the BC structure. The variation in the range and intensity of the peaks may be attributed to the

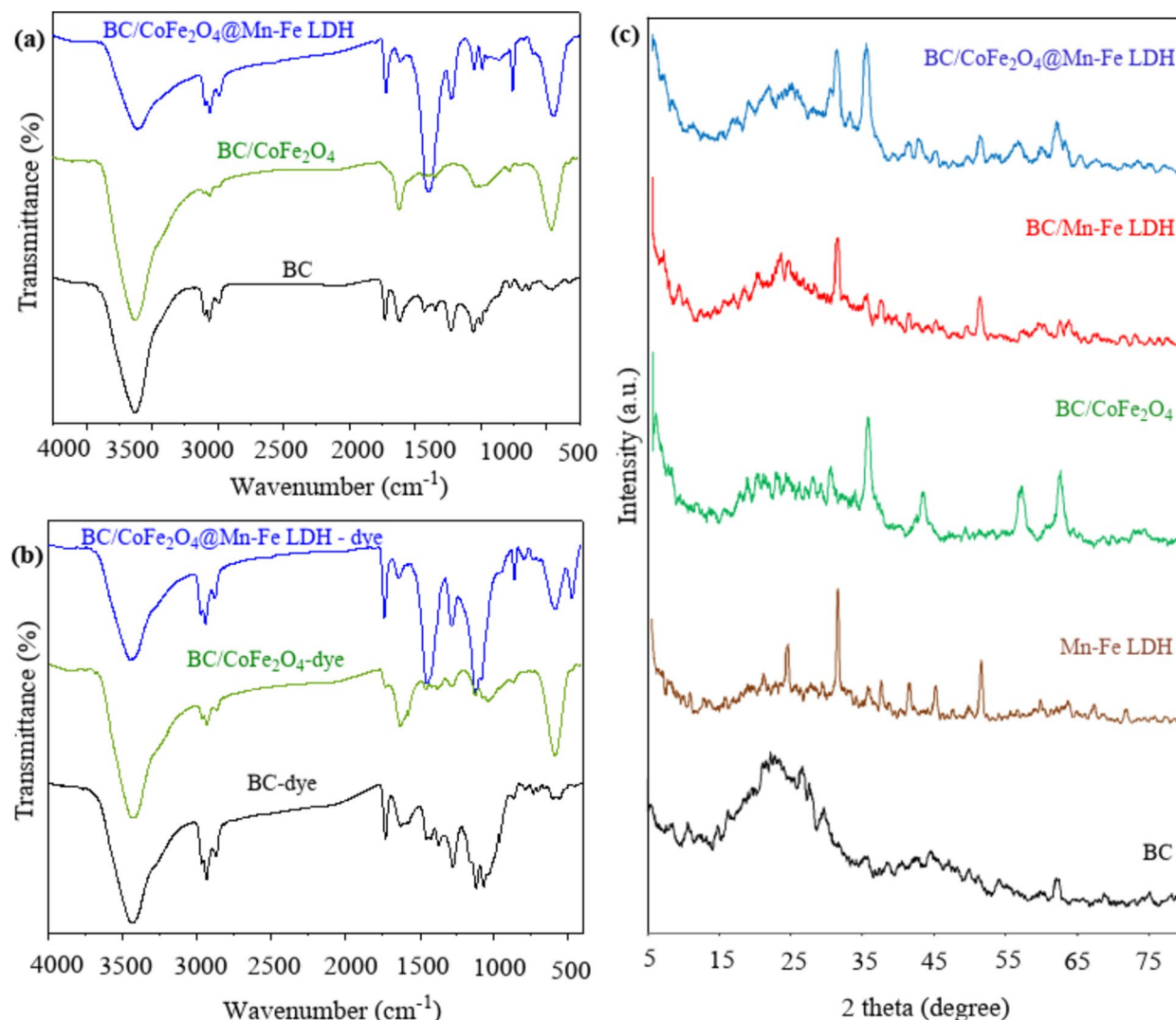


Fig. 1. FTIR analysis for BC, BC/CoFe₂O₄, and BC/CoFe₂O₄@Mn-Fe, LDH samples (a) before and (b) after CV dye adsorption process and (c) XRD spectra for BC, Mn-Fe LDH, BC/CoFe₂O₄, BC/Mn-Fe LDH, and BC/CoFe₂O₄@Mn-Fe LDH adsorbent.

arrangement of different components. After synthesizing the BC/CoFe₂O₄@Mn-Fe LDH nanocomposite, the peaks corresponding to each element are seen together, indicating the successful synthesis of the desired sample.

BET analysis is a common analytical technique used to investigate the active surface area, distribution, and size of pores in the structure of solid material, for which nitrogen adsorption-desorption isotherms were performed for BC, Mn-Fe LDH, BC/CoFe₂O₄ and BC/CoFe₂O₄@Mn-Fe LDH samples (Fig. 2). The results show that BC, Mn-Fe LDH, BC/CoFe₂O₄ and BC/CoFe₂O₄@Mn-Fe LDH samples exhibit a type IV isotherm according to the IUPAC standard, which indicates the presence of mesopores and nanometer-sized pores in their structure⁴³. In addition, the specific active surface area for BC, Mn-Fe LDH, BC/CoFe₂O₄ and BC/CoFe₂O₄@Mn-Fe LDH samples was determined to be 43.41, 95.81, 150.77, and 98.85 m²/g, respectively, which indicates that the active sites on the surface of BC sample were increased by modifying it with CoFe₂O₄ and Mn-Fe LDH. On the other hand, the average pore volume for BC, Mn-Fe LDH, BC/CoFe₂O₄, and BC/CoFe₂O₄@Mn-Fe LDH samples was determined to be 0.037, 0.22, 0.24, and 0.19 cm³/g, respectively. As can be seen, the average pore volume in the nanocomposite sample has decreased compared to BC/CoFe₂O₄, which may indicate the presence of Mn-Fe LDH particles in the structure of the sample. It is important to note that the average pore volume in the BC/CoFe₂O₄@Mn-Fe LDH sample is higher than that of BC, which could positively affect adsorption. In addition, the pore size in all samples is between 2 and 50 nm, which emphasizes that the pores are mesoporous.

Magnetic properties play an essential role in the adsorbents' effectiveness in adsorption, as they increase their economic efficiency and facilitate their separation from water and wastewater. Therefore, VSM analysis was conducted to assess the magnetic properties of the CoFe₂O₄, BC/CoFe₂O₄, and BC/CoFe₂O₄@Mn-Fe LDH samples, and the results are shown in Fig. 3, which show that the samples have magnetic behavior similar to ferromagnetic materials⁴⁴. The magnetic saturation values (*M_s*) for CoFe₂O₄ as well as BC/CoFe₂O₄ and BC/CoFe₂O₄@Mn-Fe LDH nanocomposites were determined to be 119.6, 46.45, and 32.34 emu/g, respectively. It is

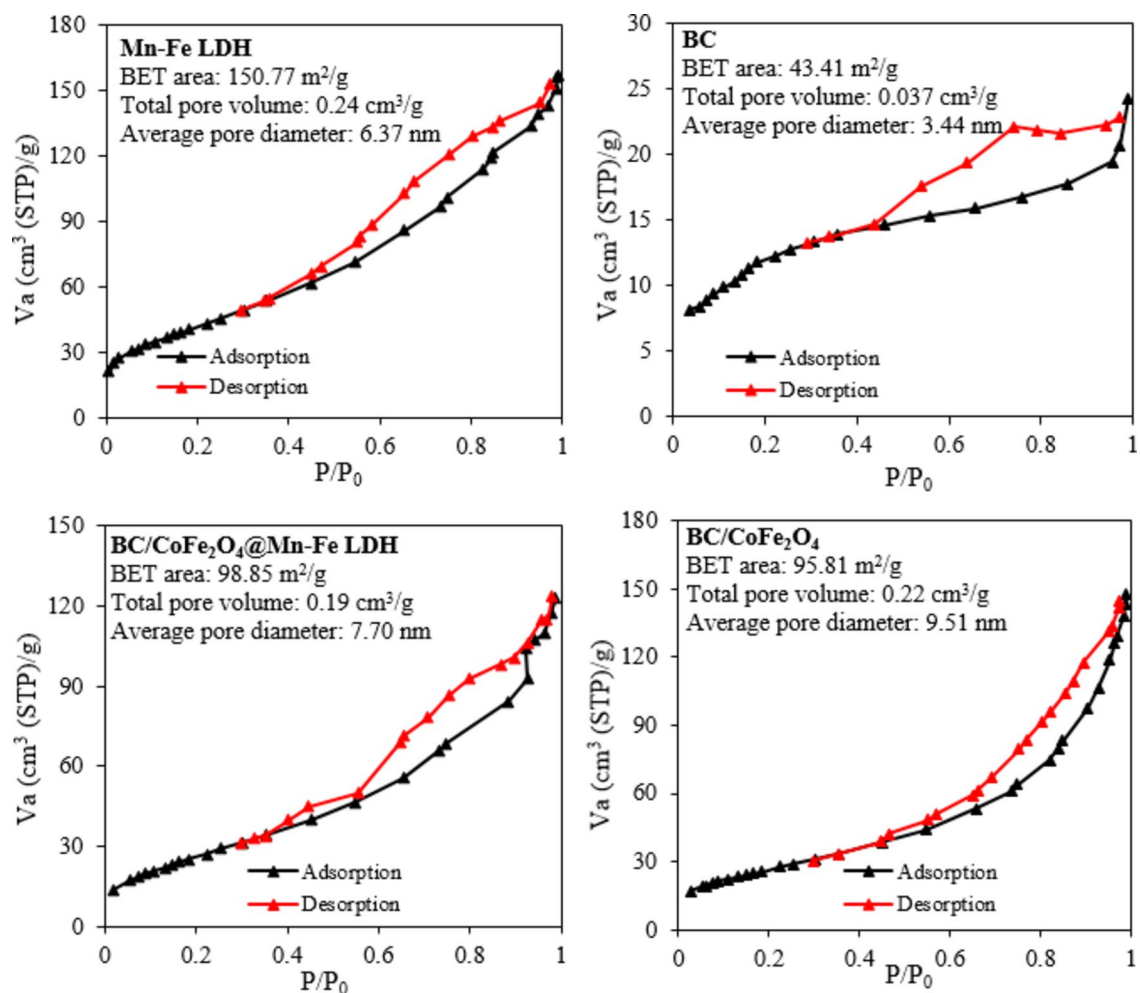


Fig. 2. BET analysis for BC, BC/CoFe₂O₄, Mn-Fe LDH, and BC/CoFe₂O₄@Mn-Fe LDH samples.

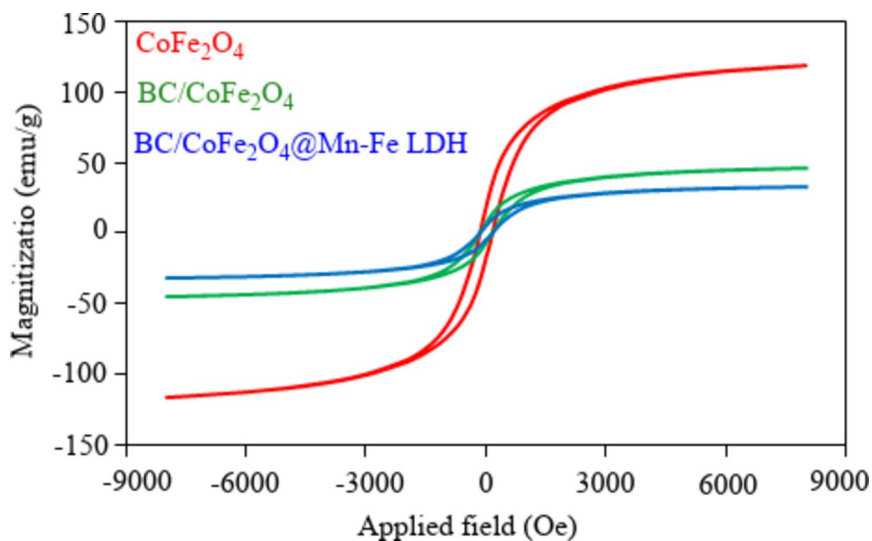


Fig. 3. VSM analysis for CoFe₂O₄, BC/CoFe₂O₄, and BC/CoFe₂O₄@Mn-Fe LDH samples.

worth mentioning that the decrease in the M_s parameter value in BC/CoFe₂O₄ and BC/CoFe₂O₄@Mn-Fe LDH samples can be attributed to several factors, including the distribution of different cations within the spinel structure, the increase in surface-to-volume ratio, random spin canting on the surface⁴⁵, and the presence of non-magnetic components in BC and Mn-Fe LDH⁴⁶. However, due to the suitable magnetic properties of the samples, a magnet can be used to separate the samples from the aqueous solution.

SEM and mapping-EDX analysis were used to investigate the morphology and surface changes of BC, BC/CoFe₂O₄, and BC/CoFe₂O₄@Mn-Fe LDH samples. The results are presented in Fig. 4. As can be seen in the presented results, the BC sample has a heterogeneous surface with smooth parts, which can be due to the pyrolysis process (Fig. 4A). In addition, mapping-EDX analysis showed that the BC sample consists of carbon (77.14 wt%) and oxygen (22.86 wt%). These elements are uniformly distributed on the sample's surface (Fig. 4B, C). After modifying the BC sample with CoFe₂O₄ magnetic nanoparticles, changes were observed on its surface, with small particles forming, likely due to the deposition of magnetic nanoparticles on the BC surface (Fig. 4D). To verify this, mapping-EDX analysis was performed. The results confirmed the presence of Fe and Co elements on the BC surface (Fig. 4E, F). Following the modification of the BC/CoFe₂O₄ magnetic nanocomposite with Mn-Fe LDH, the density of spherical particles on the surface increased, which can be attributed to the incorporation of Mn-Fe LDH (Fig. 4G). Also, mapping-EDX analysis confirmed the presence of Mn, Fe, and Co ions, indicating that Mn-Fe LDH was successfully placed in the sample's structure (Fig. 4H, I). Therefore, the presented results showed that the BC/CoFe₂O₄@Mn-Fe LDH magnetic nanocomposite was successfully synthesized using the chemical deposition method and has an irregular and heterogeneous surface.

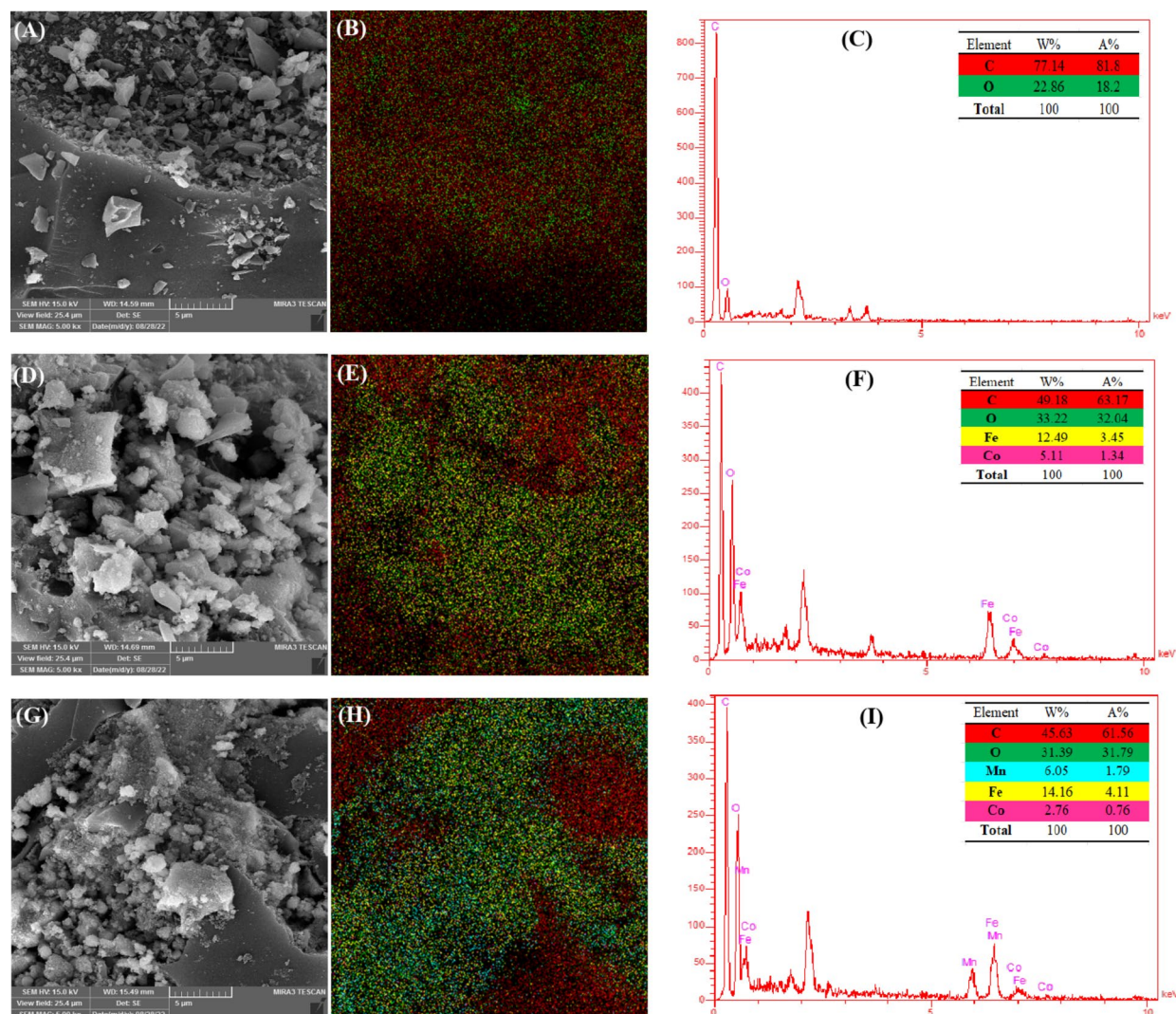


Fig. 4. SEM-EDX-Map analysis for (A–C) BC, (D–F) BC/CoFe₂O₄, and (G–I) BC/CoFe₂O₄@Mn-Fe LDH samples.

Investigation the adsorption parameters

Effect of pH and adsorbent dosage

The solution's initial pH is a key factor influencing the adsorption process, as it alters the adsorbent's surface charge and impacts the adsorption efficiency. In this study, the effect of pH changes in the range of 2–9 was examined under laboratory conditions of 25 °C, a contact time of 70 min, a dye concentration of 10 mg/L, and an adsorbent dose of 1 g/L for BC, BC/CoFe₂O₄, and BC/CoFe₂O₄@Mn-Fe LDH samples, with the results shown in Fig. 5a. The findings indicate that the adsorption efficiency increased as the pH rose from 2 to 9. At lower pH, the low adsorption rate of CV dye can be attributed to the presence of H⁺ ions, which compete with the dye molecules for active sites on the adsorbent, preventing the dye from binding effectively⁴⁷. Conversely, as pH increases, the concentration of OH⁻ in the solution rises, making the adsorbent surface more negative. This enhances the electrostatic attraction between the CV dye molecules and the adsorbent, thereby improving adsorption⁴⁸.

Another factor influencing the adsorption process is the adsorbent dose. Therefore, the effect of varying the adsorbent dose in the range of 0.5–4 g/L was investigated under laboratory conditions of 25 °C, a contact time of 70 min, a dye concentration of 10 mg/L, and pH = 9 for BC, BC/CoFe₂O₄, and BC/CoFe₂O₄@Mn-Fe LDH samples, with the results shown in Fig. 5b. The experimental results revealed that as the adsorbent dose increased within the ranges of 0.5–2, 0.5–1.5, and 0.5–1 g/L for the respective adsorbents, the adsorption efficiency improved from 48.26 to 95.62%, 54.72 to 96.63%, and 62.78 to 98.54%. The increase in CV dye adsorption efficiency with higher adsorbent doses can be attributed to the increased availability of active sites and a larger surface area on the adsorbent^{49,50}. It is important to note that after the mentioned values for each adsorbent, the changes in CV dye adsorption efficiency were insignificant, so these values were chosen as the optimal values for the adsorption process.

Effect of dye concentration CV and isotherm studies

To assess the impact of pollutant concentration on the adsorption process efficiency, CV dye concentrations ranging from 10 to 50 mg/L were chosen under constant laboratory conditions of 25 °C temperature, 70 min contact time, pH = 9, and adsorbent dosages of 2 g/L for BC, 1.5 g/L for BC/CoFe₂O₄, and 1 g/L for BC/CoFe₂O₄@Mn-Fe LDH. The results indicated that as dye concentration increased, the adsorption efficiency of these samples decreased (Fig. 6a). Specifically, the adsorption efficiency for BC, BC/CoFe₂O₄, and BC/CoFe₂O₄@Mn-Fe LDH samples decreased from 95.62, 96.63, and 98.54% to 53.63, 61.19, and 79.38%, respectively, within the concentration range of 10–50 mg/L. The higher adsorption efficiency at lower concentrations may be attributed to the greater availability of active sites on the adsorbent relative to the number of dye molecules. In contrast, the reduced adsorption efficiency at higher dye concentrations could be due to decreased available active sites for adsorption.

In the current study, the adsorption isotherms of CV dye from aqueous solutions using BC, BC/CoFe₂O₄, and BC/CoFe₂O₄@Mn-Fe, LDH samples were investigated by applying the Langmuir, Freundlich, and Temkin isotherm models. The corresponding linear equations for these models are presented in Eqs. (3–5), respectively:

$$\frac{C_e}{q_e} = \frac{C_e}{q_m} + \frac{1}{K_L q_m} \quad R_L = \frac{1}{1 + K_L C_0} \quad (3)$$

$$\ln q_e = \ln K_F + \frac{1}{n} \ln C_e \quad (4)$$

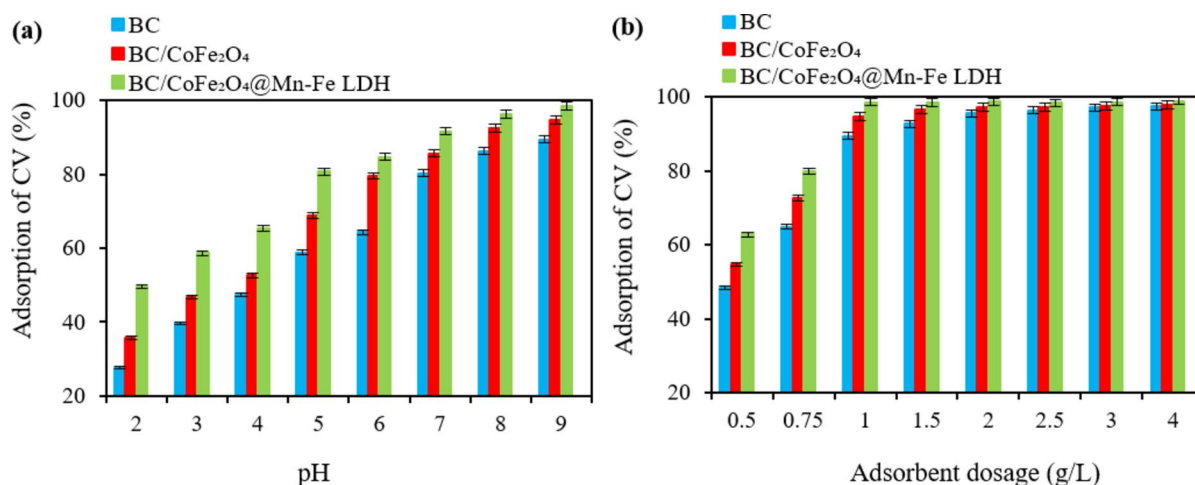


Fig. 5. (a) Impact of pH on the adsorption efficiency (temperature: 25 °C, contact time: 70 min, initial dye concentration: 10 mg/L, adsorbent dose: 1 g/L), (b) Influence of adsorbent dose on the adsorption efficiency (pH = 9, temperature: 25 °C, contact time: 70 min, initial dye concentration: 10 mg/L).

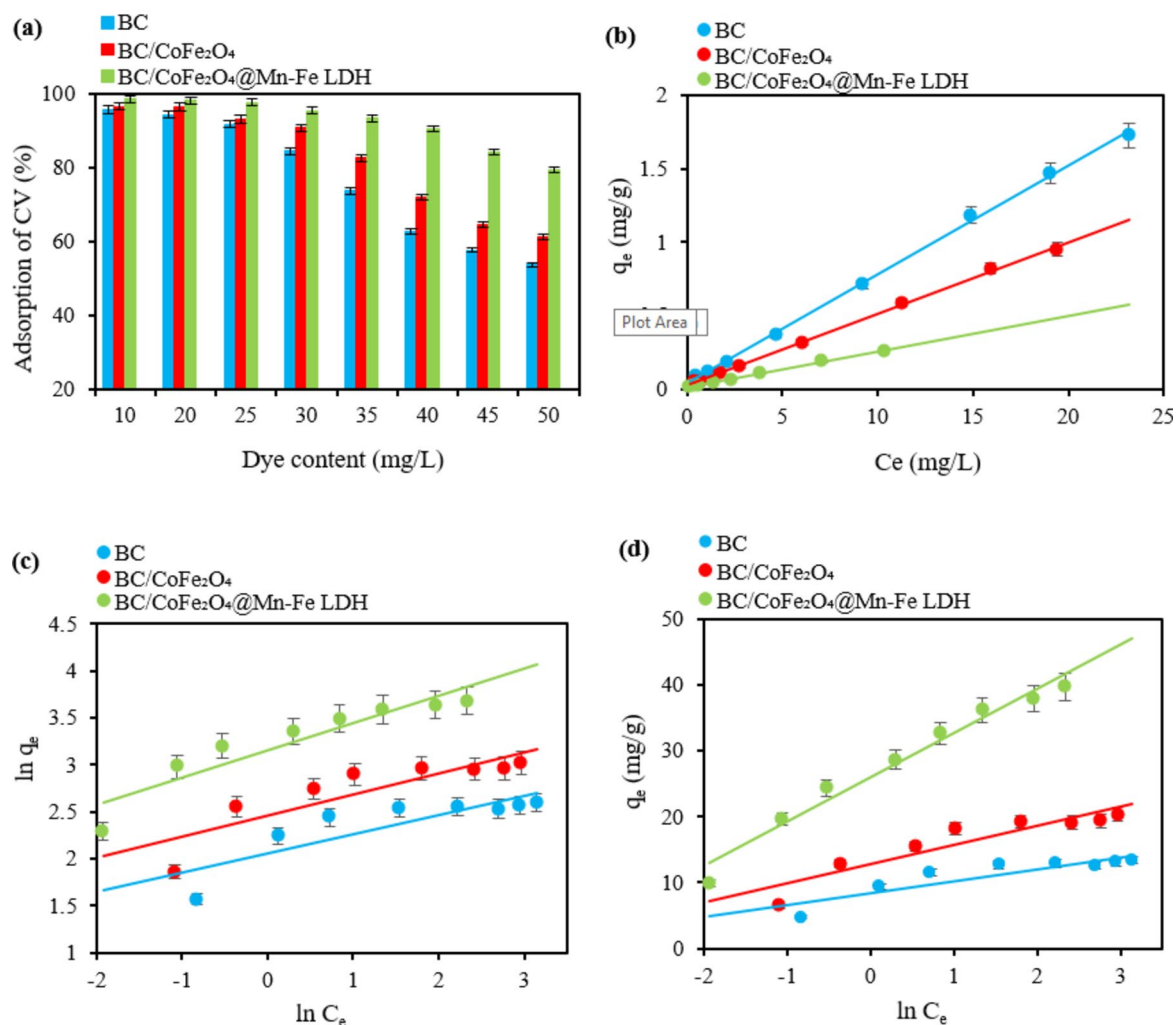


Fig. 6. (a) Effect of initial dye concentration (pH = 9, temperature 25 °C, contact time 70 min, and adsorbent dosages of 2, 1.5, and 1 g/L for BC, BC/CoFe₂O₄, and BC/CoFe₂O₄@Mn-Fe LDH samples, respectively), (b–d) Linear correlations of the Langmuir, Freundlich, and Temkin isotherm models for the CV dye adsorption process.

$$q_e = B \ln A_T + B \ln C_e \quad B = \frac{RT}{b_T} \quad (5)$$

Here, C_e represents the equilibrium concentration of CV dye in the aqueous solution (mg/L), q_m is the maximum Langmuir adsorption capacity (mg/g), K_L is the Langmuir adsorption constant, R_L is the separation factor, K_F is the Freundlich constant, n is the adsorption intensity, b_T is the Temkin isotherm constant (L/g), R is the universal gas constant (kJ/mol), A_T and b_T are the Temkin isotherm constants (kJ/mol) associated with the energy parameter, and T represents the absolute temperature (K).

The linear regression of Langmuir, Freundlich, and Temkin models are shown in Fig. 6b–d, respectively, and their related parameters are presented in Table 1. Based on the experimental data, the correlation coefficient Langmuir model (R^2) for the CV dye adsorption process using BC, BC/CoFe₂O₄, and BC/CoFe₂O₄@Mn-Fe LDH samples was determined to be 0.9987, 0.9987, and 0.9993, respectively, which is higher than that of the Freundlich model. Therefore, it can be noted that the Langmuir model has a more remarkable ability to describe the equilibrium behavior of the adsorption process, and the mechanism of the CV dye adsorption process is monolayer, and there is no intermolecular interaction⁵¹. The values of K_L and K_F for CV dye adsorption using BC/CoFe₂O₄@Mn-Fe LDH magnetic nanocomposite were determined to be 2.025 L/mg and 23.516 mg/g (L.mg)^{1/n}, respectively, which are higher than those of BC and BC/CoFe₂O₄ samples, confirming the ability and high affinity of BC/CoFe₂O₄@Mn-Fe LDH magnetic nanocomposite in CV dye adsorption⁵². It is also important to note that the R_L and n values for CV dye adsorption using the specified samples were between $0 < R_L < 1$ and greater than 1, respectively, indicating that the adsorption process is favorable and physical^{53,54}. Also, the value of $n > 1$ suggests that the active sites in the desired adsorbents' interact with more than one CV dye molecule during the adsorption process⁵⁵. Additionally, the b_T parameter for adsorption of CV dye using BC, BC/CoFe₂O₄, and

Model	Parameters	Adsorbent		
		BC	BC/CoFe ₂ O ₄	BC/CoFe ₂ O ₄ @Mn-Fe LDH
Langmuir	K _L (L/mg)	1.841	1.837	2.025
	q _m (mg/g)	13.477	20.533	41.152
	R _L	0.0107–0.0515	0.0107–0.0516	0.0097–0.047
	R ²	0.9987	0.9987	0.9993
Freundlich	K _F (mg/g (L/mg) ^{1/n})	7.845	11.713	23.516
	n	4.923	4.448	3.453
	R ²	0.7136	0.7496	0.8665
Temkin	b _T (kJ/mol)	1.383	0.848	0.367
	A _T (L/g)	111.919	77.836	46.483
	R ²	0.7936	0.849	0.9689

Table 1. Isotherm parameters obtained from the isotherm models for the CV dye adsorption process using the desired adsorbents.

Adsorbents	q _e (mg/g)	References
CAPP	17.61	57
Pumice	6.99	58
Diatom <i>Skeletonema costatum</i>	6.410	59
Almond shells	1.075	60
SBC	49.0	61
Chinar leaf powder	25.8	62
Chinar leaf biochar	30.1	62
KM 20	23.64	63
KM 40	31.35	63
Mesoporous silica particles	26.53	64
SDBS	38.16	65
BC	13.477	This study
BC/CoFe ₂ O ₄	20.533	This study
BC/CoFe ₂ O ₄ @Mn-Fe LDH	41.152	This study

Table 2. Comparison of the adsorption capacity of the desired adsorbents with other adsorbents used to remove CV dye from aqueous solution.

BC/CoFe₂O₄@Mn-Fe LDH samples was found to be 1.383, 0.848, and 0.367 kJ/mol, respectively. These values are below 8 kJ/mol, confirming that the adsorption process and the interaction between the adsorbent surface and CV dye are physical⁵⁶. Also, the adsorption capacity of CV dye was determined using BC, BC/CoFe₂O₄, and BC/CoFe₂O₄@Mn-Fe LDH samples as 13.477, 20.533, and 41.152 mg/g, respectively. In addition, the adsorption capacity of the aforementioned samples was compared with other adsorbents used in the previous study, and the results are presented in Table 2. The results showed that the adsorbents in question have the ability and appropriate adsorption capacity to remove CV dye from an aqueous solution.

Temperature effect and thermodynamic studies

Temperature plays a crucial role in the adsorption process as it influences the mobility and solubility of dye molecules in water, as well as the surface properties of the adsorbent⁶⁶. Consequently, the effect of temperature in the range of 25–50 °C was examined under laboratory conditions, with a pH of 9, an initial dye concentration of 10 mg/L, a contact time of 70 min, and adsorbent dosages of 2, 1.5, and 1 g/L for BC, BC/CoFe₂O₄, and BC/CoFe₂O₄@Mn-Fe LDH samples, respectively. The results presented in Fig. 7a showed that increasing the temperature in BC, BC/CoFe₂O₄, and BC/CoFe₂O₄@Mn-Fe LDH samples led to a decrease in the efficiency of CV dye adsorption process from 95.62, 96.63, and 98.54% to 83.54, 87.93, and 90.76%, respectively. This reduction in efficiency suggests the exothermic nature of the adsorption process. It can be attributed to the increased likelihood of the adsorbed CV dye detaching from the solid surface and re-entering the liquid phase. It also reflects the weakening of physical bonds between the dye molecules and the active sites on the adsorbent, as well as a decrease in the availability of active sites at elevated temperatures^{41,67}.

To conduct thermodynamic studies on the CV dye adsorption process, three parameters, enthalpy (ΔH°), entropy (ΔS°), and Gibbs free energy (ΔG°), were examined to assess spontaneity, determine whether the process is endothermic or exothermic, and evaluate feasibility within the temperature range of 25–50 °C, using Eqs. (6–7), respectively:

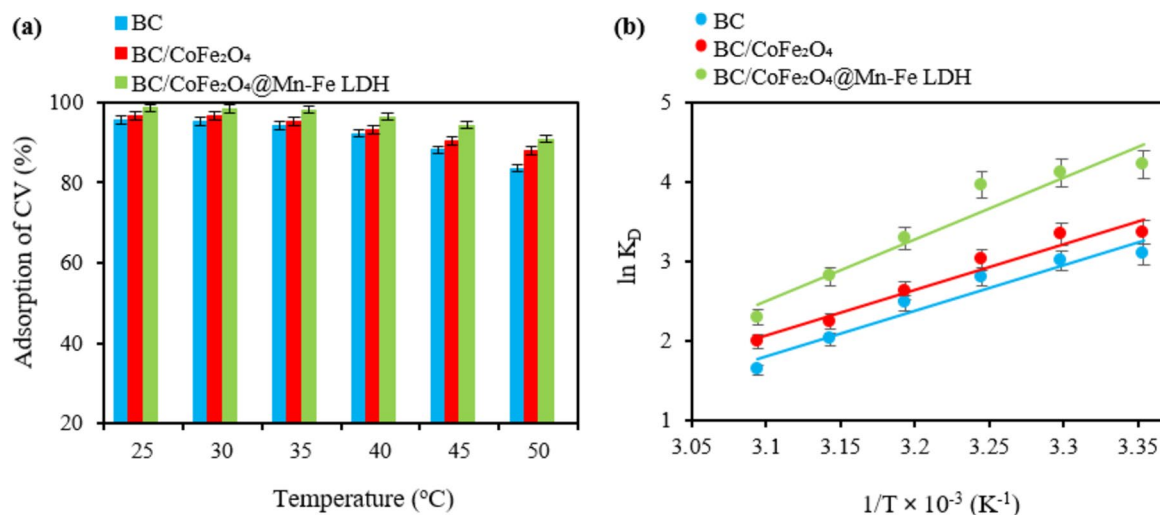


Fig. 7. (a) Effect of reaction temperature (pH = 9, initial dye concentration of 10 mg/L, contact time of 70 min, and adsorbent dosages of 2, 1.5, and 1 g/L for BC, BC/CoFe₂O₄, and BC/CoFe₂O₄@Mn-Fe LDH samples, respectively), (b) Linear relationship of $\ln K_D$ versus $1/T$ for determining thermodynamic parameters.

Adsorbent	Temperature (°C)	ΔG° (kJ/mol)	ΔH° (kJ/mol)	ΔS° (J/mol.K)
BC	25	− 7.643	− 48.131	− 134.296
	30	− 7.551		
	35	− 7.155		
	40	− 6.423		
	45	− 5.323		
	50	− 4.364		
BC/CoFe ₂ O ₄	25	− 8.318	− 48.138	− 132.143
	30	− 8.412		
	35	− 7.721		
	40	− 6.823		
	45	− 5.913		
	50	− 5.335		
BC/CoFe ₂ O ₄ @Mn-Fe LDH	25	− 10.441	− 64.724	− 179.906
	30	− 10.349		
	35	− 10.132		
	40	− 8.529		
	45	− 7.412		
	50	− 6.144		

Table 3. Thermodynamic variables determined for CV dye adsorption using the desired adsorbents.

$$\Delta G^\circ = -RT \ln K_D \quad (6)$$

$$\ln K_D = \frac{\Delta S^\circ}{R} - \frac{\Delta H^\circ}{RT} \quad (7)$$

In this context, R represents the universal gas constant, T denotes the absolute temperature (K), and K_D is the equilibrium constant for the adsorption process, calculated as the ratio of C_A , the quantity of dye adsorbed on the adsorbent surface (mg/g), to C_e , the amount of dye remaining in the aqueous solution (mg/g).

The linear regression of $\ln K_D$ versus $1/T$ for the CV dye adsorption process using the desired adsorbents is shown in Fig. 7b, and the constants and variables determined using it are presented in Table 3. As can be seen, the value of the ΔG° parameter changes in the temperature range of 25–50 °C was negative, indicating that the adsorption process is spontaneous and that low temperatures are more favorable for the adsorption process. It is important to note that the ΔG° parameter has been reported to vary between 0 and − 20 kJ/mol, confirming the physical nature of the CV dye adsorption process using the specified adsorbents under the given experimental conditions⁶⁸. Additionally, the ΔH° values for the CV dye adsorption process with BC, BC/CoFe₂O₄, and BC/CoFe₂O₄@Mn-Fe LDH were found to be − 48.131, − 48.138, and − 64.724 kJ/mol, respectively, indicating that

the process is exothermic and that the adsorption efficiency decreases as temperature increases⁶⁹. Also, the ΔS° parameter value for the CV dye adsorption using the desired adsorbents was determined to be negative, which indicates that random interactions decreased during the adsorption process, and the positioning of CV dye molecules on the surface of the adsorbents was driven by ion exchange interactions occurring throughout the adsorption process⁷⁰.

Effect of equilibration time and kinetic studies

The effect of reaction time, ranging from 5 to 100 min, on the adsorption efficiency of CV dye was studied *in vitro* at pH=9, an initial dye concentration of 10 mg/L, a temperature of 25 °C, and adsorbent dosages of 2, 1.5, and 1 g/L for BC, BC/CoFe₂O₄, and BC/CoFe₂O₄@Mn-Fe LDH samples, respectively (Fig. 8a). The studies showed that with increasing time from 5 min to 80 min for BC, BC/CoFe₂O₄, and BC/CoFe₂O₄@Mn-Fe LDH samples, the adsorption efficiency of CV dye increased from 28.56, 41.53 and 48.63% to 97.14, 98.42 and 99.28%, respectively, which could be attributed to the increased availability of active sites on the adsorbent⁷¹. After the mentioned time, with the gradual filling of the adsorption sites, there was no significant change in the process, which could be due to the saturation of the adsorbent surfaces with CV dye molecules³. Since there were no significant changes in the surface adsorption process for the BC and BC/CoFe₂O₄ samples after 80 min and for the BC/CoFe₂O₄@Mn-Fe LDH magnetic nanocomposite after 60 min, these values were chosen as the optimal reaction time.

After examining the effect of contact time, the results were used to analyze the kinetics of the CV dye adsorption process with the selected adsorbents. In this study, the pseudo-first-order (PFO), pseudo-second-order (PSO), and intra-particle diffusion kinetic models were applied to investigate the kinetic behavior of the CV dye adsorption process, and their linear relationships are given in Eqs. (8–10), respectively:

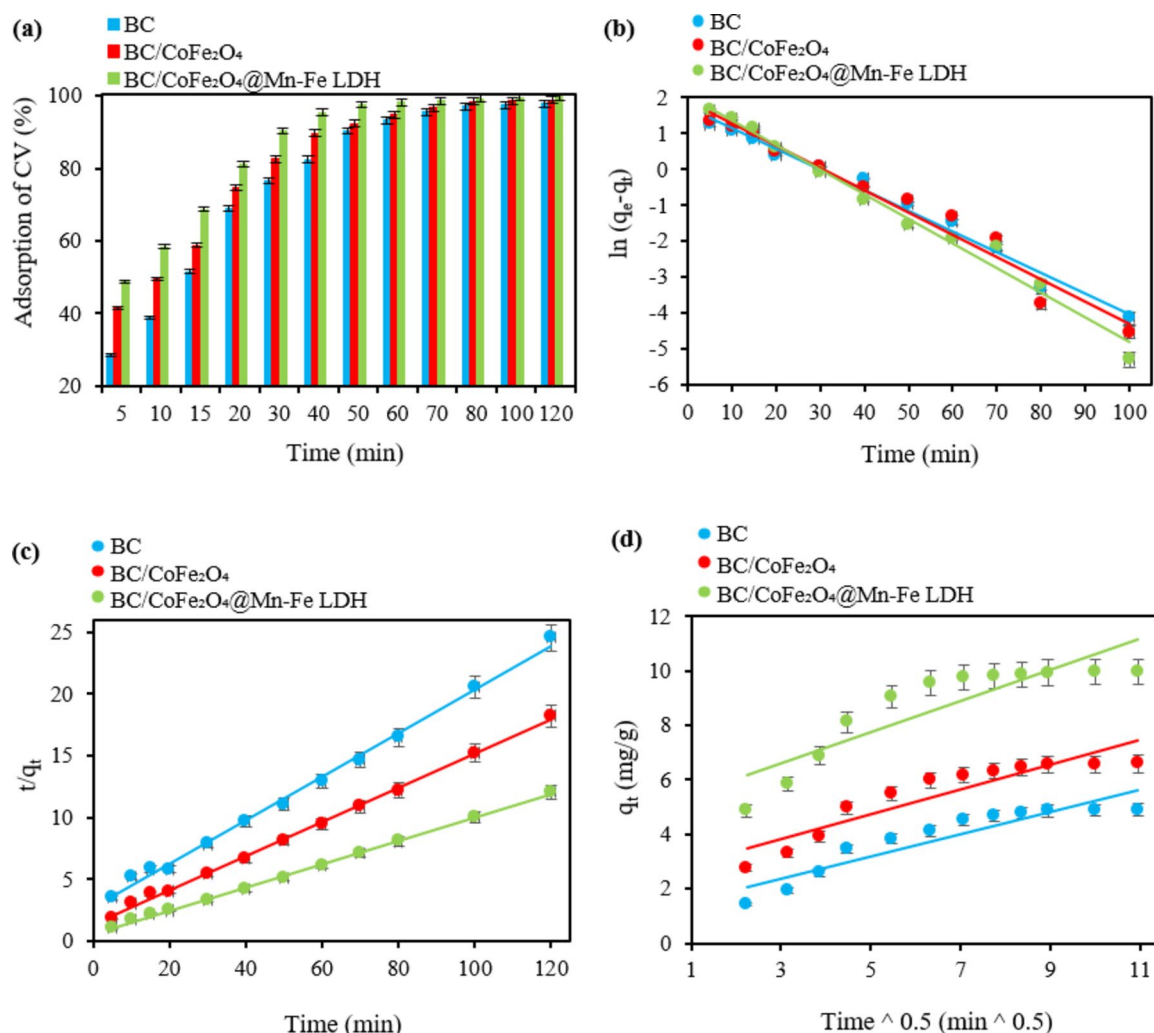


Fig. 8. (a) Effect of reaction time (pH=9, temperature 25 °C, and adsorbent dosages of 2, 1.5, and 1 g/L for BC, BC/CoFe₂O₄, and BC/CoFe₂O₄@Mn-Fe LDH samples, respectively), and the linear relationships for (b) PFO, (c) PSO, and (d) intra-particle diffusion kinetic models for CV dye adsorption using the selected adsorbents.

$$\ln (q_e - q_t) = \ln q_{e,cal} - k_1 t \tag{8}$$

$$\frac{t}{q_t} = \frac{1}{k_2 q_{e,cal}^2} + \frac{t}{q_e} \tag{9}$$

$$q_t = k_{int} \sqrt{t} + C \tag{10}$$

The linear regression of the mentioned kinetic models is shown in Fig. 8b-d, respectively, and the parameters obtained from the kinetic models for the CV dye adsorption process are presented in Table 4. Based on the experimental results, the R^2 value obtained from the PSO kinetic model for CV dye adsorption was higher than that from the PFO kinetic model, suggesting that the PSO model is more effective for describing the CV dye adsorption kinetic behavior. This implies that the rate-limiting step in the CV dye adsorption process may involve valence forces, such as electron sharing or exchange, between the adsorbent and the dye molecules⁷². Additionally, the k_2 value for CV dye adsorption using the BC/CoFe₂O₄@Mn-Fe LDH magnetic nanocomposite was higher than that for the other adsorbents, indicating that this magnetic nanocomposite has a stronger affinity for CV dye adsorption compared to the different materials⁷³. The results suggest that the intra-particle diffusion model plot is nonlinear within the studied time range, implying that the CV dye adsorption process using the selected adsorbents is influenced by multiple factors. It likely involves the mass transfer of CV dye molecules to both the external and internal surfaces of the adsorbents⁷⁴. Therefore, the fundamental mechanisms governing the adsorption process of CV dye with these adsorbents may involve film and pore diffusion, highlighting the complex nature of the adsorption mechanism⁷⁵.

Effect of counter ions and ad(de)sorption

In real conditions, aqueous solutions and wastewater obtained from different industries can contain other components in dissolved or suspended form, such as metal ions, organic materials, and microorganisms⁷⁶; therefore, In this study, KCl and CaCl₂ solutions with concentrations ranging from 0.05 to 0.5 mg/L were used as electrolyte solutions under optimal laboratory conditions, including a pH of 9, an initial dye concentration of 10 mg/L, a temperature of 25 °C, a contact time of 80 min, and adsorbent dosages of 2, 1.5, and 1 g/L for BC, BC/CoFe₂O₄, and BC/CoFe₂O₄@Mn-Fe LDH samples, respectively (Fig. 9a-b). The results show that increasing concentrations of Ca²⁺ and K⁺ ions decreases the efficiency of the adsorption process in BC, BC/CoFe₂O₄, and BC/CoFe₂O₄@Mn-Fe LDH samples. The reduction in efficiency may be attributed to the occupation of the adsorbent's active sites by counter ions, which prevents the formation of bonds between the dye molecules and the adsorbent⁷⁷. On the other hand, cations inhibit the adsorption reaction due to their larger hydration radius and electron shielding effect⁷⁸. In addition to this decrease, the efficiency of CV dye adsorption in the presence of Ca²⁺ is higher than that of K⁺, which may be attributed to the smaller ionic radius of Ca²⁺. Cations with larger ionic radii tend to have less impact on adsorption⁷⁹.

Another parameter that can be effective in the adsorption process and affect the economic cost of the pollutant removal process from aqueous solution is the regeneration-reuse of the desired adsorbent. In this regard, the ability to reuse the BC, BC/CoFe₂O₄, and BC/CoFe₂O₄@Mn-Fe LDH samples in CV dye removal up to 8 steps was studied, and the results are presented in Fig. 9c. For this purpose, first, the CV dye adsorption process was carried out using BC, BC/CoFe₂O₄ and BC/CoFe₂O₄@Mn-Fe LDH under optimal conditions. After the mentioned time, the desired adsorbents were separated from the aqueous solution and washed using deionized water. After that, the desired adsorbent was immersed in 20 mL of 0.05 M HNO₃ solution for 60 min. After the mentioned time, the separated desired adsorbents were washed using deionized water and after drying at 100 °C, they were used again in the adsorption process. As the results show, with increasing number of regeneration-reuse steps, the efficiency and performance of the desired adsorbents in CV dye removal decreases. The decrease in efficiency of CV dye adsorption process using the desired adsorbents can be attributed to saturation of the adsorbent active sites, physical damage to the adsorbent⁸⁰, incomplete removal of CV dye from adsorbent active sites⁸¹, destruction of the adsorbent surface structure and consequently reduction in adsorption capacity⁸².

Kinetic model	Parameter	Adsorbent		
		BC	BC/CoFe ₂ O ₄	BC/CoFe ₂ O ₄ @Mn-Fe LDH
PFO	q _{e,experimental}	4.893	6.584	9.968
	q _{e,calculate}	5.581	6.681	7.874
	k ₁	0.0576	0.062	0.0688
	R ²	0.9846	0.9673	0.9843
PSO	q _{e,experimental}	4.893	6.584	9.968
	q _{e,calculate}	5.656	7.231	10.626
	k ₂	0.0117	0.0143	0.0153
	R ²	0.9957	0.9981	0.9987
Intra-particle diffusion	k _{int}	0.028	0.031	0.0383
	C ₁	2.4249	3.8741	6.7188
	R ²	0.7146	0.6964	0.6163

Table 4. Kinetic variables determined for CV dye adsorption using the desired adsorbents.

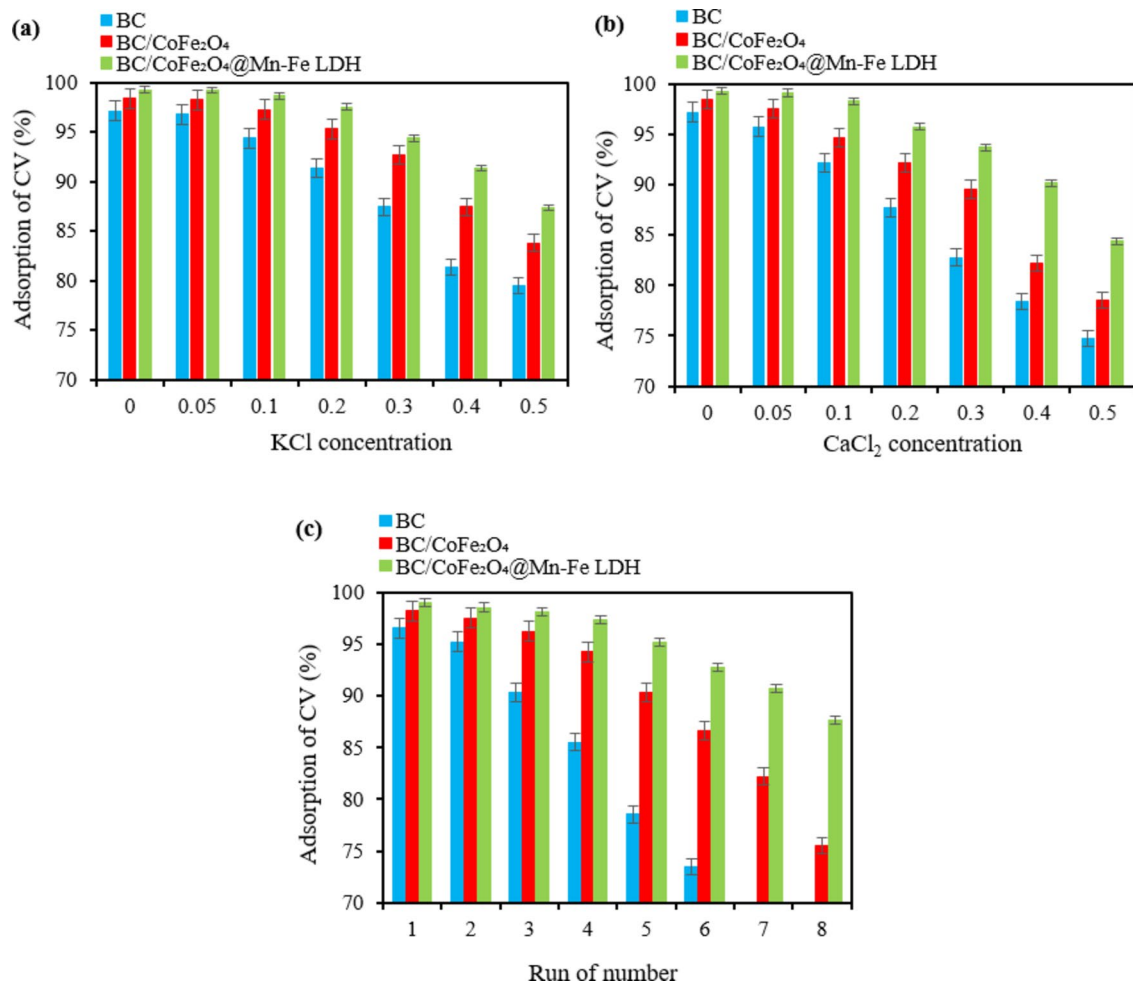


Fig. 9. Effect of counter ions of (a) potassium, and (b) calcium in aqueous solution on the CV dye removal efficiency using BC, BC/CoFe₂O₄ and BC/CoFe₂O₄@Mn-Fe LDH adsorbent samples, (c) Effect of ad(de)sorption (pH = 9, temperature 25 °C, time 80 min, initial dye concentration of 10 mg/L, and adsorbent dosages of 2, 1.5, and 1 g/L for BC, BC/CoFe₂O₄, and BC/CoFe₂O₄@Mn-Fe LDH samples, respectively.

However, it is worth noting that the CV dye removal efficiency using BC/CoFe₂O₄ and BC/CoFe₂O₄@Mn-Fe LDH is more than 90% up to 5 steps and 7 steps, respectively. This indicates that BC/CoFe₂O₄ and BC/CoFe₂O₄@Mn-Fe LDH have excellent mechanical properties of adsorbents as well as high resistance to chemical agents³³, and can be used several times in the CV dye adsorption process.

Adsorption mechanism

In the present study, the effective mechanism of the CV dye removal process using BC/CoFe₂O₄@Mn-Fe LDH sample has been thoroughly analyzed according to the results of pH, BET, FTIR, and previous studies. As we know, CV dye is a cationic dye that has higher adsorption in alkaline environments with pH results. When the pH of the aqueous solution increases, the functional groups in the adsorbent structure become surface charged, which can create an electrostatic interaction of attraction type with CV dye molecule with positive surface charge. In previous studies, electrostatic interaction has also been stated as an effective mechanism in the CV dye adsorption process¹⁶. In addition, FTIR results showed that the structure of the BC/CoFe₂O₄@Mn-Fe LDH sample contains Fe-OH, Mn-OH, Fe-O, C=O, -CH₂, and O-H functional groups that can form hydrogen bonds with the N and H groups in the CV dye structure and cause its removal from aqueous solution, which has also been proven in a previous study^{17,18}. Also, BET results showed that the BC/CoFe₂O₄@Mn-Fe LDH sample has a porous structure that can be a suitable site for the adsorption and placement of the CV dye molecule. In addition, in the structure of the BC/CoFe₂O₄@Mn-Fe LDH sample, there are functional groups containing oxygen that can form n- π interactions with the aromatic rings in the CV dye structure¹⁹ and cause the removal of the desired dye. Figure 10 shows the mechanisms effective in removing CV dye using the BC/CoFe₂O₄@Mn-Fe LDH sample.

Conclusion

The BC/CoFe₂O₄@Mn-Fe LDH magnetic nanocomposite, synthesized from pine cone-derived biochar, proved an effective adsorbent for removing the cationic dye crystal violet (CV). With a specific surface area of 98.85 m²/g

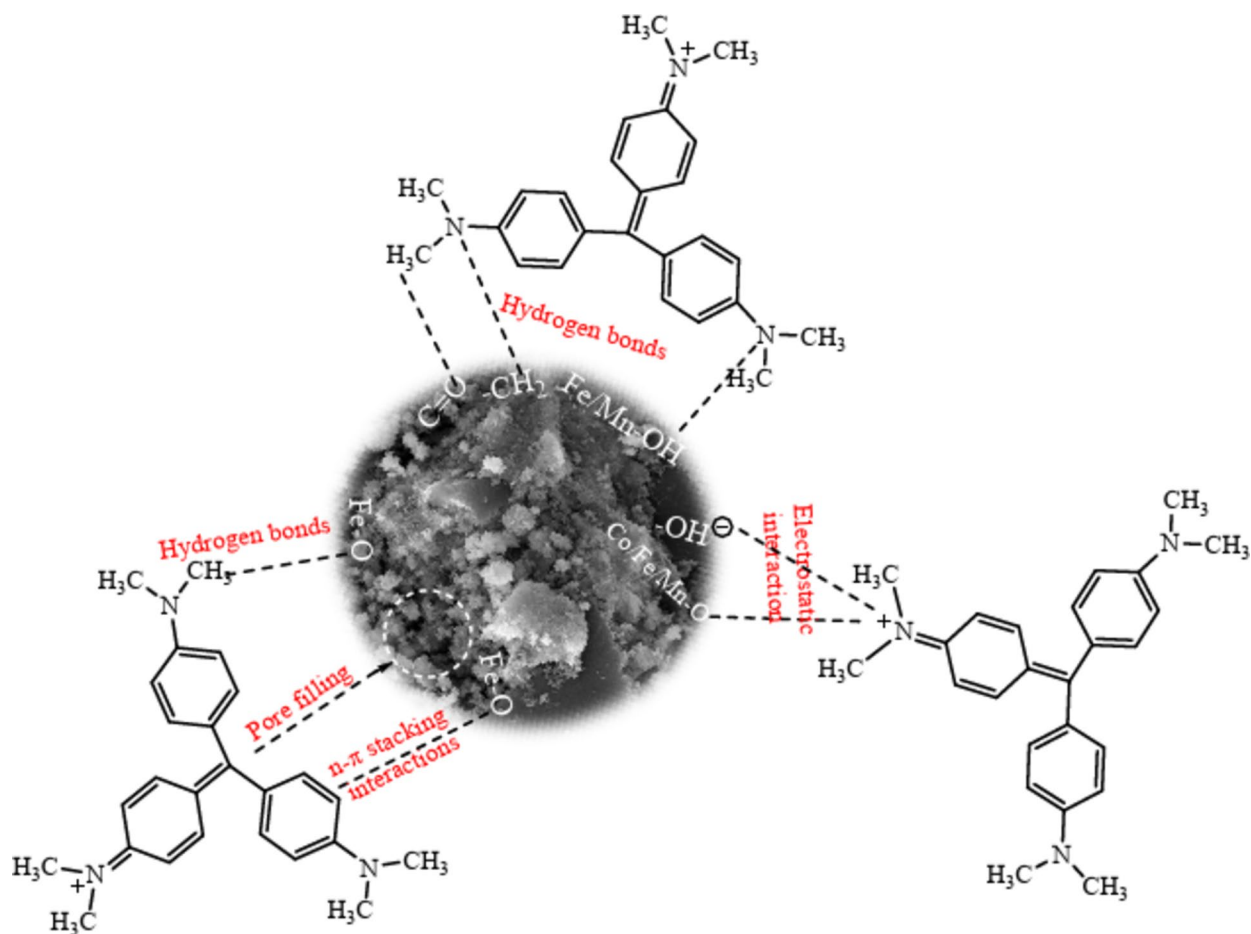


Fig. 10. Possible interactions between BC/CoFe₂O₄@Mn-Fe LDH sample with CV dye.

and magnetic saturation of 32.34 emu/g, the composite can be easily separated from the solution using an external magnet post-adsorption. The highest dye removal efficiency of 98.21% was achieved under optimal conditions (pH=9, 25 °C, 10 mg/L CV dye concentration, 1 g/L adsorbent dose, and 70 min contact time). The Langmuir isotherm model best describes adsorption, indicating monolayer adsorption on homogeneous surfaces. The negative ΔG° values suggest the adsorption process is spontaneous and physical, while the negative ΔH° and ΔS° values highlight the exothermic nature of the process and a decrease in randomness during adsorption. The pseudo-second-order kinetic model accurately captured the adsorption kinetics, underscoring the importance of physical and chemical interactions. The study also demonstrated that the presence of K⁺ and Ca²⁺ ions negatively affected adsorption efficiency, suggesting the need for optimizing water chemistry in practical applications. Overall, the BC/CoFe₂O₄@Mn-Fe LDH nanocomposite shows significant potential for dye removal from aqueous solutions, with high efficiency, magnetic separation capability, and reusability advantages.

Data availability

Data availability All data generated or analyzed during this study are included in this published article.

Received: 9 January 2025; Accepted: 21 April 2025

Published online: 29 April 2025

References

- Lebkiri, I. et al. Investigation of the anionic polyacrylamide as a potential adsorbent of crystal Violet dye from aqueous solution: equilibrium, kinetic, thermodynamic, DFT, MC and MD approaches. *J. Mol. Liq.* **372**, 121220. <https://doi.org/10.1016/j.molliq.2023.121220> (2023).
- Essekri, A., Laabd, M. & Albourine, A. Efficient adsorption of crystal Violet dye using functionalized Argan shell: experiments and statistical optimization modeling. *Colloids Surf., A* **687**, 133401. <https://doi.org/10.1016/j.colsurfa.2024.133401> (2024).
- Kumbhar, P. et al. Synthesis of tea waste/Fe₃O₄ magnetic composite (TWMC) for efficient adsorption of crystal Violet dye: isotherm, kinetic and thermodynamic studies. *J. Environ. Chem. Eng.* **10**(3), 107893. <https://doi.org/10.1016/j.jece.2022.107893> (2022).
- Komal, R. C., Srivastava, C. S., Joshi & Verma, H. K. Zinc oxide and nickel ferrite nanocomposite as an efficient photocatalyst for crystal Violet dye degradation. *Solid State Commun.*, **386**, 115517. <https://doi.org/10.1016/j.ssc.2024.115517> (2024).

5. Raji, Y. et al. High adsorption capacities of crystal Violet dye by low-cost activated carbon prepared from Moroccan Moringa oleifera wastes: characterization, adsorption and mechanism study. *Diam. Relat. Mater.* **135**, 109834 (2023).
6. Peighambari, S. J. et al. Effectiveness of polyacrylamide-g-gelatin/ACL/Mg-Fe LDH composite hydrogel as an eliminator of crystal Violet dye. *Environ. Res.* **258**, 119428. <https://doi.org/10.1016/j.envres.2024.119428> (2024).
7. Rath, J. et al. Green synthesis of silver nanoparticles decorated on graphene oxide for crystal Violet dye removal. *Diam. Relat. Mater.* **146**, 111192. <https://doi.org/10.1016/j.diamond.2024.111192> (2024).
8. Yilmazoglu, M., Kanmaz, N. & Demirci, P. Constructing the synergistic effects of Chitosan and ionic liquid on SPEEK polymer for efficient adsorption of crystal Violet dye. *Int. J. Biol. Macromol.* **271**, 132638. <https://doi.org/10.1016/j.ijbiomac.2024.132638> (2024).
9. Veni, K. K., Nehru, L. C., Kavitha, R. & Sagadevan, S. Synergistic effect of sonophotocatalytic degradation of crystal Violet and Alizarin red S dyes using Ag-doped ZnSnO₃ nanoparticles. *Surf. Interfaces*, **51**, 104590. <https://doi.org/10.1016/j.surfint.2024.104590> (2024).
10. Allahkarami, E., Dehghan Monfared, A., Silva, L. F. O. & Dotto, G. L. Lead ferrite-activated carbon magnetic composite for efficient removal of phenol from aqueous solutions: synthesis, characterization, and adsorption studies. *Sci. Rep.* **12** (1), 10718 (2022).
11. Allahkarami, E., Monfared, A. D. & Karri, R. R. Chapter 5 - Activated carbon adsorbents for the removal of emerging pollutants and its adsorption mechanisms. In *Sustainable Remediation Technologies for Emerging Pollutants in Aqueous Environment*, M. Hadi Dehghani, and I. Tyagi Eds.: Elsevier, 79–109. (2024).
12. Thamer, B. M., Al-aizari, F. A., Abdo, H. S. & Al-Enizi, A. M. Activated carbon-decorated electrospun polystyrene fibers for highly efficient removal of hazardous crystal Violet dye from water. *Colloids Surf., A*, **688**, 133612. <https://doi.org/10.1016/j.colsurfa.2024.133612> (2024).
13. Chinoune, K. et al. Adsorption behavior of MB dye on alginate-sepiolite biocomposite beads: Adsorption, kinetics, and modeling. *Inorg. Chem. Commun.* **165**, 112558. <https://doi.org/10.1016/j.inoche.2024.112558> (2024).
14. Osagie, C. et al. Dyes adsorption from aqueous media through the nanotechnology: A review. *J. Mater. Res. Technol.* **14**, 2195–2218. <https://doi.org/10.1016/j.jmrt.2021.07.085> (2021).
15. Saini, P., Chakinala, N., Surolia, P. K. & Gupta Chakinala, A. Ultrasound-assisted enhanced adsorption of textile dyes with metal organic frameworks. *Sep. Purif. Technol.*, **354**, 128730. <https://doi.org/10.1016/j.seppur.2024.128730> (2025).
16. Chebbi, M., Ounoki, S., Youcef, L., Chergui, F. N. & Amrane, A. Sustainable pine cone adsorbent: removal of prednisolone and pre-treatment of a medical lab wastewater. *Sustainable Chem. Pharm.* **39**, 101565. <https://doi.org/10.1016/j.scp.2024.101565> (2024).
17. Song, Y., Ma, M., Su, Q., Du, Y. & Du, D. The new strategy of using pine-cone Biochar to enhance anaerobic digestion of liquor wastewater for methane production. *J. Clean. Prod.*, **438**, 140748. <https://doi.org/10.1016/j.jclepro.2024.140748> (2024).
18. Mokubung, K. E., Gumbi, N. N., Lau, W. J. & Nxumalo, E. N. Pine cone derived polyethersulfone/biochar-Fe₃O₄ mixed matrix membranes for removal of arsenic from acid mine drainage. *Chem. Eng. Res. Des.* **201**, 31–44. <https://doi.org/10.1016/j.cherd.2023.11.010> (2024).
19. Chebbi, M., Ounoki, S., Youcef, L. & Amrane, A. Synthesis and characterization of pine cones Biochar for the removal of an antibiotic (Metronidazole) from aqueous solutions. *J. Ind. Eng. Chem.* **126**, 327–339. <https://doi.org/10.1016/j.jiec.2023.06.023> (2023).
20. Jari, Y. et al. Porous activated carbons derived from waste Moroccan pine cones for high-performance adsorption of bisphenol A from water. *Heliyon* **10**, 9 (2024).
21. Bık, J. & Kolodyńska, D. Synthesis and study of the sorption potential of hydrotalcite modified biochars (LDH@BC) with respect to cerium(III) ions. *Chem. Eng. J.* **494**, 152888. <https://doi.org/10.1016/j.cej.2024.152888> (2024).
22. Yang, Q. et al. In situ stabilization of the adsorbed Co²⁺ and Ni²⁺ in rice straw Biochar based on LDH and its reutilization in the activation of peroxymonosulfate. *J. Hazard. Mater.*, **416**, 126215. <https://doi.org/10.1016/j.jhazmat.2021.126215> (2021).
23. Li, S. et al. Adsorption and mechanistic study of the invasive plant-derived Biochar functionalized with CaAl-LDH for Eu (III) in water. *J. Environ. Sci.* **96**, 127–137 (2020).
24. Fan, S. et al. KOH activated Biochar loaded with MnAl-layered double hydroxides for superior adsorption of Tetracycline from the aquatic environment. *J. Ind. Eng. Chem.*, **134**, 474–483. <https://doi.org/10.1016/j.jiec.2024.01.010> (2024).
25. Li, B. et al. Complexation between Butyl Xanthate and Cu enhanced peroxydisulfate activation and cation redox cycle by Fe-Cu-LDH/biochar. *J. Environ. Chem. Eng.* **12**(2), 112466. <https://doi.org/10.1016/j.jece.2024.112466> (2024).
26. Miao, J., Zhao, X., Zhang, Y. X. & Liu, Z. H. Feasible synthesis of hierarchical porous MgAl-borate LDHs functionalized Fe₃O₄@SiO₂ magnetic microspheres with excellent adsorption performance toward congo red and Cr(VI) pollutants. *J. Alloys Compd.*, **861**, 157974. <https://doi.org/10.1016/j.jallcom.2020.157974> (2021).
27. Lu, L. et al. Synthesis of novel hierarchically porous Fe₃O₄@MgAl-LDH magnetic microspheres and its Superb adsorption properties of dye from water. *J. Ind. Eng. Chem.*, **46**, 315–323. <https://doi.org/10.1016/j.jiec.2016.10.045> (2017).
28. Zare, M. R. et al. Adsorption of acid red 18 from aqueous solutions by GO-COFe₂O₄: adsorption kinetic and isotherms, adsorption mechanism and adsorbent regeneration. *Desalination Water Treat.* **317**, 100219. <https://doi.org/10.1016/j.dwt.2024.100219> (2024).
29. Zeng, Y., Xie, J., Xiao, X., Chen, L. & Zhu, X. Synthesis of CoFe₂O₄@SiO₂-NH₂ and its application in adsorption of trace lead. *RSC Adv.* **14** (1), 589–601 (2024).
30. Foroutan, R., Peighambari, S. J., Hemmati, S., Khatooni, H. & Ramavandi, B. Preparation of clinoptilolite/starch/CoFe₂O₄ magnetic nanocomposite powder and its elimination properties for cationic dyes from water and wastewater. *Int. J. Biol. Macromol.* **189**, 432–442. <https://doi.org/10.1016/j.ijbiomac.2021.08.144> (2021).
31. Abbasi, M., Sabzehmeidani, M. M., Ghaedi, M., Jannesar, R. & Shokrollahi, A. Synthesis of grass-like structured Mn-Fe layered double hydroxides/pes composite adsorptive membrane for removal of malachite green. *Appl. Clay Sci.* **203**, 105946. <https://doi.org/10.1016/j.clay.2020.105946> (2021).
32. Khan, B. A. et al. Adsorption and immobilization performance of pine-cone pristine and engineered biochars for antimony in aqueous solution and military shooting range soil: an integrated novel approach. *Environ. Pollut.*, **317**, 120723. <https://doi.org/10.1016/j.envpol.2022.120723> (2023).
33. Hu, X. et al. Comparison study on the ammonium adsorption of the biochars derived from different kinds of fruit Peel. *Sci. Total Environ.*, **707**, 135544. <https://doi.org/10.1016/j.scitotenv.2019.135544> (2020).
34. Subratti, A., Vidal, J. L., Lalgue, L. J., Kerton, F. M. & Jalsa, N. K. Preparation and characterization of biochar derived from the fruit seed of Cedrela odorata L and evaluation of its adsorption capacity with methylene blue. *Sustain. Chem. Pharm.* **21**, 100421. <https://doi.org/10.1016/j.scp.2021.100421> (2021).
35. Mohammed, N. A. S., Abu-Zurayk, R. A., Hamadneh, I. & Al-Dujaili, A. H. Phenol adsorption on Biochar prepared from the pine fruit shells: equilibrium, kinetic and thermodynamics studies. *J. Environ. Manage.*, **226**, 377–385. <https://doi.org/10.1016/j.jenvman.2018.08.033> (2018).
36. Gotore, O. et al. Iodine adsorption isotherms on Matamba fruit shell stemmed biochar for wastewater re-use strategy in rural areas owing to climate change. *Chemosphere* **303**, 135126. <https://doi.org/10.1016/j.chemosphere.2022.135126> (2022).
37. Chakhtouna, H., Benzeid, H., Zari, N. & Bouhfid, R. A. e. k. Quiss, and Functional CoFe₂O₄-modified biochar derived from banana pseudostem as an efficient adsorbent for the removal of amoxicillin from water. *Sep. Purif. Technol.* **266**, 118592. <https://doi.org/10.1016/j.seppur.2021.118592> (2021).
38. Gong, C. et al. Heterogeneous activation of peroxymonosulfate by Fe-Co layered doubled hydroxide for efficient catalytic degradation of rhodamine B. *Chem. Eng. J.*, **321**, 222–232. <https://doi.org/10.1016/j.cej.2017.03.117> (2017).

39. Azalok, K. A., Oladipo, A. A. & Gazi, M. UV-light-induced photocatalytic performance of reusable MnFe-LDO–biochar for Tetracycline removal in water. *J. Photochem. Photobiol., A*, **405**, 112976. <https://doi.org/10.1016/j.jphotochem.2020.112976> (2021).
40. Hou, L. et al. Heterogeneous activation of peroxymonosulfate using Mn-Fe layered double hydroxide: performance and mechanism for organic pollutant degradation. *Sci. Total Environ.* **663**, 453–464. <https://doi.org/10.1016/j.scitotenv.2019.01.190> (2019).
41. Pashaei-Fakhri, S., Peighambari, S. J., Foroutan, R., Arsalani, N. & Ramavandi, B. Crystal Violet dye sorption over acrylamide/graphene oxide bonded sodium alginate nanocomposite hydrogel. *Chemosphere* **270**, 129419. <https://doi.org/10.1016/j.chemosphere.2020.129419> (2021).
42. Sabna, V., Thampi, S. G. & Chandrakaran, S. Adsorption of crystal Violet onto functionalised multi-walled carbon nanotubes: equilibrium and kinetic studies. *Ecotoxicol. Environ. Saf.*, **134**, 390–397. <https://doi.org/10.1016/j.ecoenv.2015.09.018> (2016).
43. Foroughi, M., Salem, A. & Salem, S. Potential of fusion technique in production of mesoporous zeolite A powder from poor Kaolin through modification by boehmite: effect of clay mineralogy on particle morphology. *Adv. Powder Technol.* **32** (7), 2423–2432. <https://doi.org/10.1016/j.apt.2021.05.019> (2021).
44. Zarghami Qaretepeh, M., Kouchakipour, S., Hosseinzadeh, M. & Dashtian, K. Cuttlefish Bone-Supported CoFe_2O_4 nanoparticles enhance persulfate Fenton-like process for the degradation of polystyrene nanoplastics. *Chem. Eng. J.* **490**, 151833. <https://doi.org/10.1016/j.cej.2024.151833> (2024).
45. Ajami, A., Sheibani, S. & Ataie, A. S-scheme $\text{CoFe}_2\text{O}_4/\text{g-C}_3\text{N}_4$ nanocomposite with high photocatalytic activity and antibacterial capability under visible light irradiation. *J. Mater. Res. Technol.* **30**, 2168–2185. <https://doi.org/10.1016/j.jmrt.2024.04.010> (2024).
46. Poormand, F., Farhadi, S., Zabardasti, A. & Mahmoudi, F. Construction of novel $\text{CoFe}_2\text{O}_4/\text{h-BN}/\text{MIL-53}$ (Al) magnetic nanocomposites for the removal of hazardous antibiotics from water. *Inorg. Chem. Commun.* **161**, 111978. <https://doi.org/10.1016/j.inoche.2023.111978> (2024).
47. Boukarma, L. et al. Novel insights into crystal violet dye adsorption onto various macroalgae: Comparative study, recyclability and overview of chromium (VI) removal. *Bioresour. Technol.* **394**, 130197. <https://doi.org/10.1016/j.biortech.2023.130197> (2024).
48. Azizi, N., Eslami, R., Goudarzi, S. & Zarrin, H. Harnessing synergy: Polydopamine-hBN integration in electrospun nanofibers for Co (II) ion, methylene blue and crystal violet dyes adsorption. *Chemosphere* **363**, 142842. <https://doi.org/10.1016/j.chemosphere.2024.142842> (2024).
49. Homagai, P. L., Poudel, R., Poudel, S. & Bhattarai, A. Adsorption and removal of crystal Violet dye from aqueous solution by modified rice husk, *Heliyon*, **8**, 4, (2022).
50. Tan, Q. et al. Synthesis of a novel magnetically recyclable starch-based adsorbent for efficient adsorption of crystal Violet dye. *Sep. Purif. Technol.*, **320**, 124157. <https://doi.org/10.1016/j.seppur.2023.124157> (2023).
51. Ji, L., Luo, L., Jin, D. & Qin, X. Preparation of aligned porous carbon microtubes by a reactant permeation template method and the highly selective adsorption of methylene blue dye from wastewater. *Sep. Purif. Technol.*, **332**, 125884. <https://doi.org/10.1016/j.seppur.2023.125884> (2024).
52. Patil, D. J. & Grewal, H. S. Carboxylic acid-based fuel mediated sustainable one-pot fabrication of CaFe_2O_4 with enhanced adsorptive elimination of hazardous dye. *Inorg. Chem. Commun.*, **171**, 113601. <https://doi.org/10.1016/j.inoche.2024.113601> (2025).
53. P. S. S. K. & P. S. A. S. R. Computation of adsorption parameters for the removal of dye from wastewater by microwave assisted sawdust: theoretical and experimental analysis. *Environ. Toxicol. Pharmacol.* **50**, 45–57. <https://doi.org/10.1016/j.etap.2017.01.014> (2017).
54. Allahkarami, E., Allahkarami, E., Heydari, M., Azadmehr, A. & Maghsoudi, A. Cationic dye remediation in water treatment with Lizardite–Rice husk composite: A statistical physics approach. *J. Mol. Liq.*, **414**, 126096. <https://doi.org/10.1016/j.molliq.2024.126096> (2024).
55. Allahkarami, E., Maleki, S., Azadmehr, A., Aghayan, S. & Allahkarami, E. Fabricating nepheline syenite-chitosan composite for heavy metals uptake: mechanism insight via statistical physics modeling. *Sep. Purif. Technol.*, **354**, 129152. <https://doi.org/10.1016/j.seppur.2024.129152> (2025).
56. Araújo, C. S. T. et al. Elucidation of mechanism involved in adsorption of Pb(II) onto lobeira fruit (*Solanum lycocarpum*) using Langmuir, Freundlich and Temkin isotherms. *Microchem. J.* **137**, 348–354. <https://doi.org/10.1016/j.microc.2017.11.009> (2018).
57. Khan, T. A., Rahman, R. & Khan, E. A. Decolorization of Bismarck brown R and crystal Violet in liquid phase using modified pea peels: non-linear isotherm and kinetics modeling. *Model. Earth Syst. Environ.* **2**, 1–11 (2016).
58. Shayesteh, H., Rahbar-Kelishami, A. & Norouzbegi, R. Adsorption of malachite green and crystal Violet cationic dyes from aqueous solution using pumice stone as a low-cost adsorbent: kinetic, equilibrium, and thermodynamic studies. *Desalination Water Treat.* **57** (27), 12822–12831 (2016).
59. Ashour, M., Alprol, A. E., Khedawy, M., Abualnaja, K. M. & Mansour, A. T. Equilibrium and kinetic modeling of crystal violet dye adsorption by a marine diatom, *skeletonema costatum*. *Materials* **15**(18), 6375 (2022).
60. Goksu, A. & Tanaydin, M. K. Adsorption of hazardous crystal Violet dye by almond shells and determination of optimum process conditions by Taguchi method. *Desalination Water Treat.* **88**, 189–199 (2017).
61. Sewu, D. D., Lee, D. S., Woo, S. H. & Kalderis, D. Decolorization of triarylmethane dyes, malachite green, and crystal Violet, by sewage sludge Biochar: isotherm, kinetics, and adsorption mechanism comparison. *Korean J. Chem. Eng.* **38**, 531–539 (2021).
62. Ahmad Khan, F., Ahad, A., Shah, S. S. & Farooqui, M. Adsorption of crystal Violet dye using *Platanus orientalis* (Chinar tree) leaf powder and its Biochar: equilibrium, kinetics and thermodynamics study. *Int. J. Environ. Anal. Chem.* **103** (16), 4820–4840 (2023).
63. Yap, P. S. & Priya, V. Removal of crystal violet and acid green 25 from water using kaolin. In *IOP conference series: materials science and engineering*, vol. 495, no. 1: IOP Publishing, p. 012052 (2019).
64. Naseem, T. et al. Mesoporous silica prepared via a green route: a comparative study for the removal of crystal Violet from wastewater. *Mater. Res. Express*. **8** (1), 015005 (2020).
65. Li, W. et al. Adsorption kinetics and isothermal adsorption model of crystal violet on modified red mud. In *IOP Conference Series: Earth and Environmental Science*, vol. 508, no. 1: IOP Publishing, p. 012151. (2020).
66. Cheruiyot, G. K., Wanyonyi, W. C., Kiplimo, J. J. & Maina, E. N. Adsorption of toxic crystal Violet dye using coffee husks: equilibrium, kinetics and thermodynamics study. *Sci. Afr.*, **5**, e00116. <https://doi.org/10.1016/j.sciaf.2019.e00116> (2019).
67. A. salah omer et al., Adsorption of crystal Violet and methylene blue dyes using a cellulose-based adsorbent from Sugarcane Bagasse: characterization, kinetic and isotherm studies. *J. Mater. Res. Technol.*, **19**, 3241–3254. <https://doi.org/10.1016/j.jmrt.2022.06.045> (2022).
68. Mahdavi, Z. et al. Enhancing fluoride ion removal from aqueous solutions and glass manufacturing wastewater using modified orange peel biochar magnetic composite with MIL-53. *Environ. Res.* **262**, 119825. <https://doi.org/10.1016/j.envres.2024.119825> (2024).
69. Mohammadi, N., Khani, H., Gupta, V. K., Amereh, E. & Agarwal, S. Adsorption process of Methyl orange dye onto mesoporous carbon material–kinetic and thermodynamic studies. *J. Colloid Interface Sci.*, **362**, 2, 457–462. <https://doi.org/10.1016/j.jcis.2011.06.067> (2011).
70. Nannu Shankar, S. et al. Adsorption kinetics, equilibrium and thermodynamics of a textile dye V5BN by a natural nanocomplex material: clinoptilolite. *Energy Nexus*, **10**, 100197. <https://doi.org/10.1016/j.nexus.2023.100197> (2023).
71. Gohr, M. S., Abd-Elhamid, A. I., El-Shanshory, A. A. & Soliman, H. M. A. Adsorption of cationic dyes onto chemically modified activated carbon: kinetics and thermodynamic study. *J. Mol. Liq.*, **346**, 118227. <https://doi.org/10.1016/j.molliq.2021.118227> (2022).

72. Loutfi, M., Mariouch, R., Mariouch, I., Belfaquir, M. & ElYoubi, M. S. Adsorption of methylene blue dye from aqueous solutions onto natural clay: Equilibrium and kinetic studies. *Mater. Today Proc.* **72**, 3638–3643. <https://doi.org/10.1016/j.matpr.2022.08.412> (2023).
73. Ferreira, D. C. M., dos Santos, T. C., d., J. S., Coimbra, R. & de Oliveira, E. B. Chitosan/carboxymethylcellulose polyelectrolyte complexes (PECs) are an effective material for dye and heavy metal adsorption from water. *Carbohydr. Polym.*, **315**, 120977. <https://doi.org/10.1016/j.carbpol.2023.120977> (2023).
74. Yusuff, A. S., Obende, B. A. & Egbosiuba, T. C. Photocatalytic decolorization of textile effluent over ZnO nanoparticles immobilized on eucalyptus bark Biochar: parametric optimization, kinetic and economic analyses. *Water Resour. Ind.*, **31**, 100245. <https://doi.org/10.1016/j.wri.2024.100245> (2024).
75. Hussain, S. et al. Enhanced adsorption of congo red dye by CS/PEG/ZnO composite hydrogel: synthesis, characterization, and performance evaluation. *J. Mol. Liq.*, **411**, 125704. <https://doi.org/10.1016/j.molliq.2024.125704> (2024).
76. Wu, Z. et al. Pod-inspired MXene/porous carbon microspheres with ultrahigh adsorption capacity towards crystal Violet. *Chem. Eng. J.*, **426**, 130776. <https://doi.org/10.1016/j.cej.2021.130776> (2021).
77. Yadav, S. et al. Facile Preparation of methionine-functionalized graphene Oxide/chitosan polymer nanocomposite aerogel for the efficient removal of dyes and metal ions from aqueous solutions. *Environ. Nanotechnol. Monit. Manage.*, **18**, 100743. <https://doi.org/10.1016/j.enmm.2022.100743> (2022).
78. Zhao, C. et al. Influence of multivalent background ions competition adsorption on the adsorption behavior of Azo dye molecules and removal mechanism: based on machine learning, DFT and experiments. *Sep. Purif. Technol.*, **341**, 126810. <https://doi.org/10.1016/j.seppur.2024.126810> (2024).
79. Ganji, H. & TaghaviJeloudar, M. Efficient adsorption of lead and copper from water by modification of sand filter with a green plant-based adsorbent: adsorption kinetics and regeneration. *Environ. Res.*, **259**, 119529. <https://doi.org/10.1016/j.envres.2024.119529> (2024).
80. Esseki, A. et al. The use of Raw and modified acacia leaves for adsorptive removal of crystal Violet from water. *Chem. Eng. Res. Des.*, **190**, 143–156. <https://doi.org/10.1016/j.cherd.2022.12.010> (2023).
81. Foroutan, R., Tutunchi, A., Foroughi, A. & Ramavandi, B. Defluorination of water solutions and glass industry wastewater using a magnetic pineapple hydrochar nanocomposite modified with a covalent organic framework. *J. Environ. Manage.* **377**, 124651. <https://doi.org/10.1016/j.jenvman.2025.124651> (2025). 2025/03/01/.
82. Abdelmoby, M. et al. Silver nanowires/chitosan-derived porous carbon sheets nanocomposite for the efficient removal of crystal Violet and methylene blue dyes from wastewater. *Inorg. Chem. Commun.*, **174**, 114041. <https://doi.org/10.1016/j.inoche.2025.114041> (2025).
83. Sulyman, M., Kucinska-Lipka, J., Sienkiewicz, M. & Gierak, A. Development, characterization and evaluation of composite adsorbent for the adsorption of crystal Violet from aqueous solution: isotherm, kinetics, and thermodynamic studies. *Arab. J. Chem.*, **14**(5), 103115. <https://doi.org/10.1016/j.arabjc.2021.103115> (2021).

Author contributions

Author Contribution Statement Seyed Jamaledin Peighambardoust designed the study, interpreted the results, and revised the manuscript critically for important intellectual content; Shima Abdollahian Aghbolagh performed the samples' synthesis and collected test data; Rauf Foroutan drafted and advised on conceptualization of the manuscript; and Naeimeh Sadat Peighambardoust advised on conceptualization. All authors approve the final version of the manuscript and agree to be accountable for all aspects of the work.

Funding

This research was conducted without commercial or financial relationships that could be construed as a potential conflict of interest. The authors, therefore, declare no conflict of interest.

Declarations

Competing interests

The authors declare no competing interests.

Additional information

Correspondence and requests for materials should be addressed to S.J.P.

Reprints and permissions information is available at www.nature.com/reprints.

Publisher's note Springer Nature remains neutral with regard to jurisdictional claims in published maps and institutional affiliations.

Open Access This article is licensed under a Creative Commons Attribution-NonCommercial-NoDerivatives 4.0 International License, which permits any non-commercial use, sharing, distribution and reproduction in any medium or format, as long as you give appropriate credit to the original author(s) and the source, provide a link to the Creative Commons licence, and indicate if you modified the licensed material. You do not have permission under this licence to share adapted material derived from this article or parts of it. The images or other third party material in this article are included in the article's Creative Commons licence, unless indicated otherwise in a credit line to the material. If material is not included in the article's Creative Commons licence and your intended use is not permitted by statutory regulation or exceeds the permitted use, you will need to obtain permission directly from the copyright holder. To view a copy of this licence, visit <http://creativecommons.org/licenses/by-nc-nd/4.0/>.

© The Author(s) 2025